JAERI 1032

Measurements and Calculations for Graphite-Moderated Enriched-Fuel Critical Assembly, SHE

1962年6月

日本原子力研究所

Japan Atomic Energy Research Institute

JAERI 1032 UDC 621.039.519.4 : 621.039.524.2

MEASUREMENTS AND CALCULATIONS FOR GRAPHITE-MODERATED ENRICHED-FUEL CRITICAL ASSEMBLY, SHE*

ABSTRACT

To understand the reactor physics in enriched-fuel, graphite-moderated thermal reactors theoretical and experimental investigations have been performed. A critical assembly has been used to obtain the criticality data. An approach of criticality calculations has been developed, and it is demonstrated that the procedure is feasible in the limited area such as in the case of enriched-fuel, graphite-moderated small thermal reactors. The agreement between the theoretical and experimental criticality data is good. The effect of chemical binding in the graphite is of interest in the thermal reactor. Then the results of theoretical calculations are also presented.

January 31, 1962

K. INOUE,
M. IIZUMI
S. KOBAYASHI[i)]
K. SUMITA
Japan Atomic Energy Research Institute

黒鉛減速濃縮ウラン臨界集合体 (SHE) の実験と臨界計算*

要　旨

黒鉛減速濃縮ウラン熱中性子原子炉の炉物理に関する理解を増すために，理論および実験の両面からの研究がおこなわれた．この目的のために臨界集合体が組立てられ，臨界データの測定がおこなわれた．臨界計算の近似の組合せ方が検討され，その結果から小型の黒鉛減速濃縮ウラン熱中性子炉に対してはその方法が適していることが示された．臨界量に関する理論と実験の一致はよい．なお，黒鉛の化学結合が熱中性子炉に及ぼす効果について調べたが，その結果の一部をあわせてのべる．

1962 年 1 月

日本原子力研究所
井 上 和 彦
飯 泉　　仁
小 林 節 雄[i)]
住 田 健 二

---

* This work has been done in co-operation with the members of the group who assisted in taking the data, in maintenance and operation of the facility and in the theoretical calculation; K. NISHIMURA[ii)], S. MATSUURA, I. KOBAYASHI, Y. KANEKO, K. HIGUCHI, F. KUROSAWA,[iii)], K. KATORI[iii)], and T. W. PARK[iv)] were especially of aid in experimental work, and N. SHIRAI[ii)] in carrying out the theoretical calculation.

i) Central Res. Lab., Hitachi Ltd., ii) Meiden-sha Mfg. Co., Ltd., iii) Nippon Atomic Industry Group Co., Ltd., iv) Tokai Univ.

* この研究はＳＨＥグループの協力のもとに実施され，実験データの測定，臨界集合体の運転と保守，および理論計算がおこなわれた．実験関係の仕事には西村佳寿雄[ii)]，松浦祥次郎，小林岩夫，金子義彦，樋口幸次郎，黒沢文夫[iii)]，鹿取謙二[iii)]，朴泰玩[iv)] の諸氏に負うところが多い．また理論計算は白井信行氏[ii)] の協力を得ておこなわれた．

i) 日立中央研究所，ii) 明電舎株式会社，iii) 日本原子力事業株式会社，iv) 東海大学

CONTENTS

1. Introduction

Although many experimental and theoretical studies have been made of graphite-moderated, natural-uranium reactors, for a graphite-moderated, enriched system, there is only a limited knowledge of criticality and neutron spectrum. Enriched-fuel, graphite-moderated reactors tend to be more compact, thus the details of the neutron leakage, which depends on the neutron spectrum in the core, are important. This report describes experimental results for the graphite-moderated, enriched-fuel critical assembly and the results of the theoretical calculations used to interpret the critical data. Also a brief account of the effect of chemical binding of the graphite is given.

The critical assembly SHE, Semi-Homogeneous Experiments, was built to obtain the reactor physics data on a enriched-uranium, graphite-moderated system at room temperature. This assembly is a thermal reactor with a mixed spectrum and a relatively large fraction of resonance fissions. The experiments began in January 1961 and the experimental program on the first loaded core continued to the beginning of 1962. In order to minimize the ambiguities in interpretation of the experimental results and theoretical calculations, efforts were made to keep the assembly as simple as possible. Because of the small quantity of the fuel, the system had a relatively large reflector. The experiments were performed to determine accurately the criticality, considering the effects of the disturbing factors such as the control and safety rod channels and other poisoning structures.

The major difference between natural uranium and enriched uranium graphite-moderated reactors results from the fact that the neutron leakage from the core is much larger in the latter system than in the former. Many of the enriched-fuel, thermal reactors have a relatively small core, thus the treatment of neutron leakage is a major source of uncertainty in these reactors. The thermal reactor under consideration has a mixed spectrum in which as much as 10 to 20 percent of the total fissions result from the neutron absorption in the resonance energy region. The accuracy with which the behavior of the neutrons in the thermal reactor with a mixed spectrum can be described depends on the knowledge of the thermal neutron spectrum as well as the resonance and fast neutron spectra. The present approach includes a multigroup method to treat effectively the resonance and fast neutron spectra and a crystal model of graphite for thermal neutrons. Although theoretical treatment of spatially dependent thermal spectra should have been made in the calculation, the core was treated as being infinite in the calculation of the thermal neutron spectrum. The interaction of neutrons with the crystal lattice affects neutron thermalization. As the result, there is a need for considering the scattering law of thermal neutrons in graphite moderator. The average value of logarithmic energy loss of the scattered neutrons by graphite does fall much below the value in the case of free carbon moderator. This effect results from the fact that the allowable density of momentum states for the neutrons is less in the graphite than in the free carbon moderator. Thus in graphite moderated reactors, the thermal neutron spectrum is much hardened than in the free-carbon moderator.

Information gained from the investigation of the enriched-uranium, graphite-moderated system provides a better understanding of the physics of thermal reactors with mixed spectrum. On the other hand, the neutron spectrum information obtained in the investigation is of a general use. In particular, the knowledge obtained of the thermal neutron spectra in a graphite-moderated reactor may be applied to natural-uranium, graphite-moderated reactors, and is useful in evaluating their long-term change of reactivity and temperature coefficient.

2. Critical Assembly

The SHE critical facility is a half machine type assembly, which consists of a pile of graphite tubes and rods in hexagonal array. The central region of the pile is a matrix of tubes into which the fuel rods can be placed. Two sets of rods are provided, i. e., a set of fuel rods and a set of graphite dummy rods. Two halves are identical except that one half is moved and the other fixed. A view of the SHE facility is shown in Fig. 1.

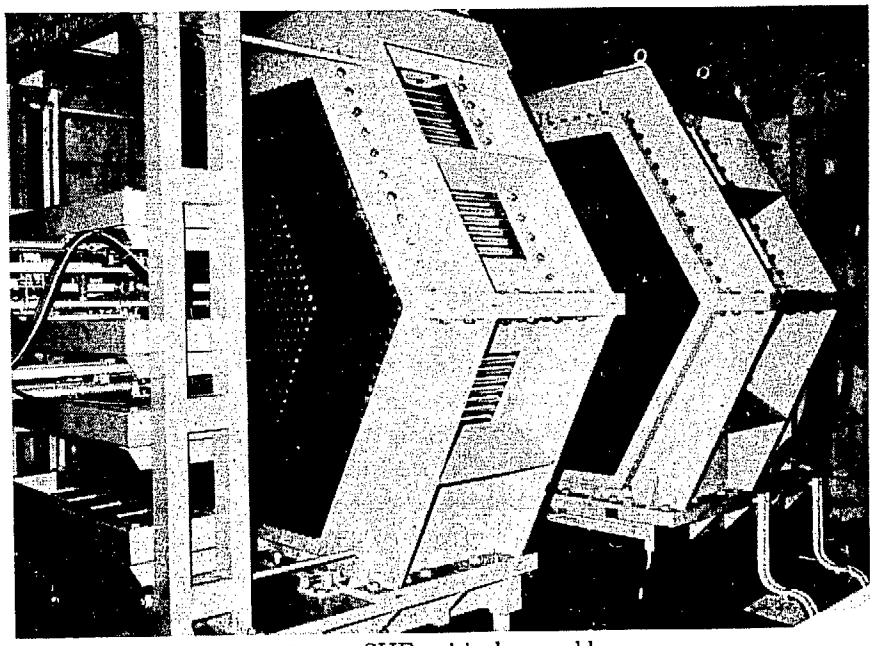

Fig. 1 SHE critical assembly

The driving speed for the moving half is slowed down near the closed position. The fast-drive speed is 50 cm/min from 150 cm to 20 cm separations, and the slow-drive is 1. 5 cm/min from 20 cm separation to the closed position. The distance between the two halves is indicated by three position indicators; one is an analogue indicator and the other two digital indicators. The position of the movable table relative to the fixed table is found to be reproducible within about 0. 01 mm at the closed position.

Two control and six safety rod mechanisms are mounted on the supporting flames behind the two halves. These control and safety rods are either cadmium or boron poisoning rods, and their full stroke is about 90 cm. The drive mechanism for the control rod consists of a D. C. motor with a drive screw and an air cylinder in which air pressure is applied to both side of the piston. The maximum drive speed by the motor is 24 cm/min, which corresponds to the rate of about 0. 01 percent per second in reactivity change. This speed may be changed and each control rod has a digital position-indicator capable within the accuracy of 0. 01 cm. The drive mechanism for the safety rod consists of an air cylinder and a magnet clutch. The outer and inner positions of the safety rod are indicated by limit switches and indicator lamps.

A radium-beryllium neutron source of about 8×10^6 neutrons per second is used as a start-up neutron source and is inserted by the drive mechanism from its coffin through a thimble to a position adjacent to the core matrix in the fixed half. The source can be withdrawn from the core into the coffin after criticality is attained.

The fuel of the SHE assembly is a homogeneous mixture of 20% enriched uranium-oxide and graphite in the form of disks of 4. 5 cm diameter and 1 cm thickness, with the graphite to uranium-

oxide weight ratio being ten. Disks of a thorium-oxide and graphite mixture as well as of pure graphite are used to vary the core composition. The physical constants of the fuel disks and graphite are shown in TABLE 1 and TABLE 2. The structure of the fuel rods is shown in Fig. 2. The outside

TABLE 1 Ingredient fuel and graphite

Uranium-oxide	
Enrichment	19.85±0.15%
O/U	2.03
Impurities B	<0.5 ppm
Cd	0.2 ppm
Al	15 ppm
Fe	30 ppm
Graphite	
Impurities B	<0.1 ppm
Ashes	<20 ppm

TABLE 2 Fuel elements

"U" disk	
Diameter	44.5 mm
Thickness	10.0 mm
Weight	34.4 g
^{235}U	0.515 g
^{238}U	2.08 g
C	29.4 g
C/UO_2 (weight ratio)	10
Density	2.1 g/cm³
Thickness of coating	<0.02 mm
Graphite disk	
Diameter	44.5 mm
Thickness	10.0 or 5.0 mm
Weight ("1" disk)	26.16 g
("5" disk)	13.04 g
Density	1.7±0.03 g/cm³
Matrix tube and fuel sheath	
Matrix tube Outer diameter	6.50 cm
Inner diameter	5.52 cm
Fuel sheath Outer diameter	5.47 cm
Inner diameter	4.52 cm
Density	1.7±0.03 g/cm³

diameter of the graphite sheath is 5.5 cm and the inside diameter 4.5 cm, and the overall length is about 120 cm. The fuel rods are placed in the core matrix in a hexagonal array. The layout of the core matrix and reflector is shown in Fig. 3 and Fig. 4 by the section through the interface. The position of each rod identified by the coordinate system is shown in Fig. 5.

The poisons in the system are the springs in the fuel rods, the tephlon coating on the fuel disks, impurities in the graphite and uranium oxide, and moisture and air in the graphite pore. Considerable uncertainty is caused by the effect of slowing down of fast neutrons by the moisture

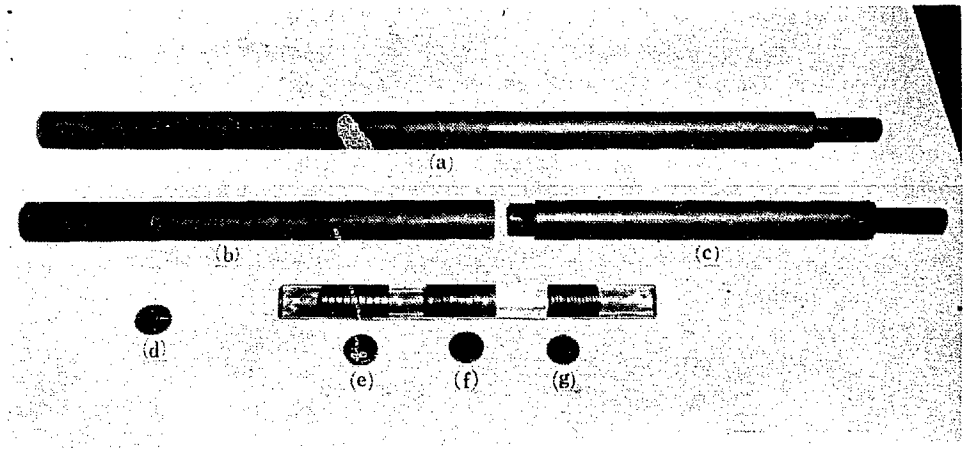

(a) Fuel rod, (b) Sheath, (c) Graphite rod which serves as a part of end reflector, (d) Plug, (e) Fuel disk. (f) 1-disk, (g) 5-disk

Fig. 2 Fuel elements

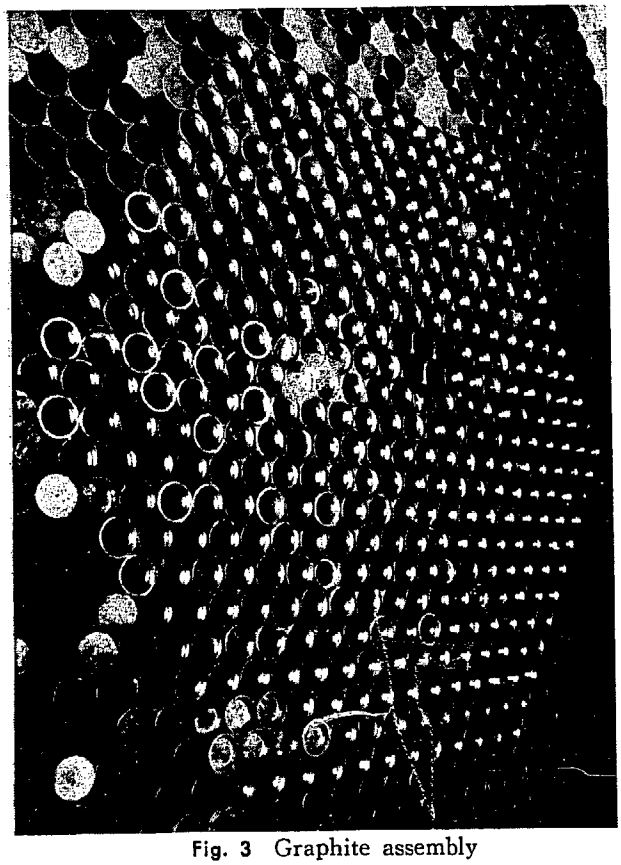

Fig. 3 Graphite assembly

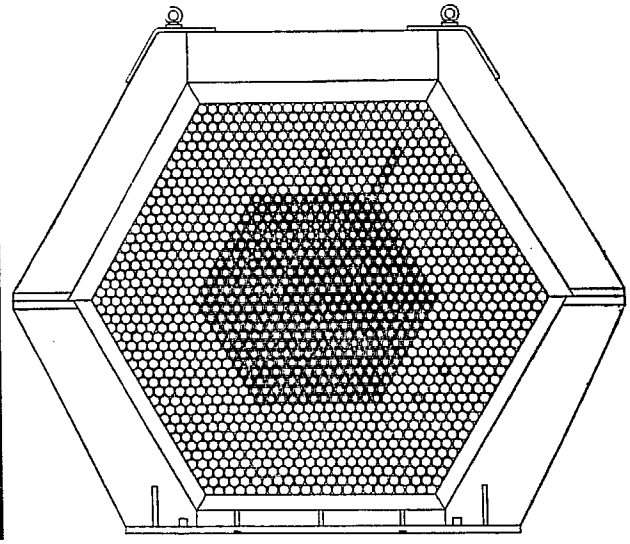

Fig. 4 Layout of SHE core

in the graphite.

The composition of the reactor is varied by the way of arrangement of the disks. In the SHE-I experiments the disk pattern consisted of a fuel disk, a 1 cm graphite and a 0.5 cm graphite disk. This pattern was repeated for the first 50 cm of the sheath, with the remaining part of the fuel rod being pure graphite. The pattern is presented symbolically by the rod pattern writing the code of the disks. In the SHE-I the rod pattern was (U15), resulting in the carbon to ^{235}U ratio of 5378. The typical pattern together with their atomic ratios and average densities is described in TABLE 3.

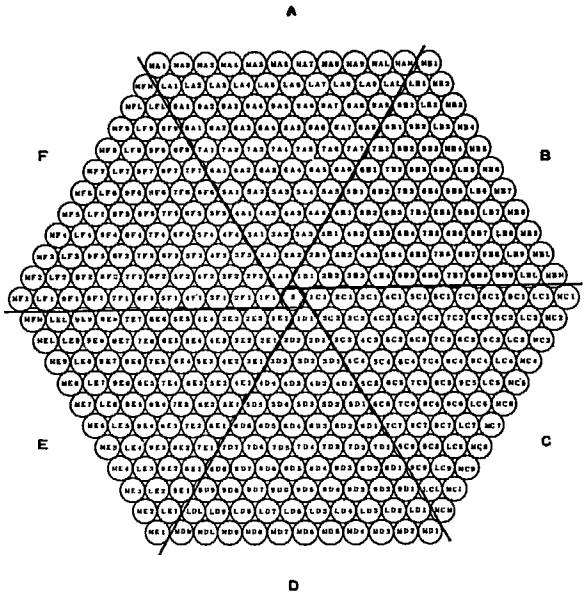

Fig. 5(a) Matrix co-ordinate (fixed half)

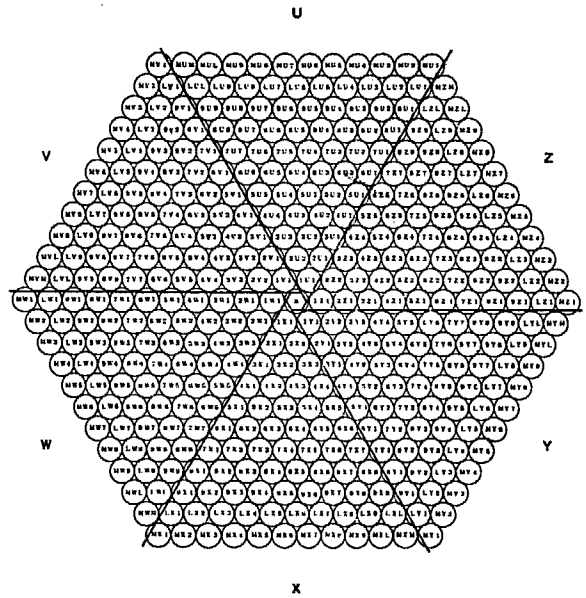

Fig. 5(b) Matrix co-ordinate (movable half)

TABLE 3 Composition of the core in various patterns

Pattern	C/^{235}U	C/^{238}U	Average densities ($\times 10^{20}$/cm^3)		
			^{235}U	^{238}U	C
(U)	2226	558.4	0.3599	1.435	801.2
(U5)	3276	821.7	0.2399	0.9565	785.9
(U1 U5)	3803	953.7	0.2056	0.8198	781.9
(U1)	4328	1086	0.1799	0.7173	778.8
(U15)	5378	1349	0.1439	0.5739	774.1
(U11)	6431	1613	0.1200	0.4782	771.4
(U115)	7480	1876	0.1028	0.4099	769.1
(U111)	8533	2140	0.08997	0.3587	767.7

3. First Loading of SHE

The matrix of the SHE core was initially filled with dummy graphite rods, and in the critical loading the dummy rods were gradually replaced by the fuel rods. The loading of the core started from the center channel and proceeded to the outer region of the core matrix. In each stage of the loading, the counting rates were observed by neutron counter channels after a batch of fuel rods was added to the core. (TABLE 4)

The assembly of the fuel rod was the arrangement of disks in the pattern already given and the insertion of the set of disks into a graphite sheath. The arrangement of the disks was made on a horizontal channel of the charging machine in a fume box. After assembly a limited number of fuel rods were carried to the reactor and replaced the dummy rods in the matrix. The loading of the fuel was so performed that at each stage the numbers of rods added to both the halves were as far close to the same number as possible.

The neutron and gamma flux levels were monitored by means of seven instruments, i. e., four ionization chambers, two BF_3 counters and a scintillation counter for gamma rays. The last approach to the criticality was performed on these channels, and the criticality was achieved with 345 fuel

TABLE 4 Counting rates of counters

(counts/min)

Loading	Control rods		Counted channel			
	Fixed side	Movable side	A	B	C	D
No loading	in	in	1727	8281	632	3205
	out	in	1776	9056	680	3292
	out	out	2453	12238	836	3601
8 th loading	in	in	11365	128038	12830	37052
	out	in	19926	227867	22430	62697
	out	out	93363	974732	98926	252636

rods, with all the safety rods and one control rod being fully withdrawn and another control rod being partially inserted.

In each stage of the loading, observation of the counting rates was made by the neutron counter channels. Four BF_3 counters were distributed throughout the boundary between the core and reflector in the positions 6A2, LAL, MBL and MC6, respectively. By using counting results, a

TABLE 5 Neutron multiplication

Loading	Number of fuel rods	Control rods		Counting channels				Average
		Fixed side	Movable side	A	B	C	D	
1	71	in	in	1.66	2.32	2.19	1.77	1.98
		out	in	1.79	2.40	2.25	1.83	2.07
		out	out	1.70	2.39	2.26	1.94	2.07
2	95	in	in	1.93	2.86	2.80	2.23	2.45
		out	in	2.06	3.02	2.82	2.21	2.53
		out	out	2.02	2.97	3.04	2.38	2.60
3	129	in	in	2.30	3.72	3.65	2.63	3.18
		out	in	2.45	3.95	3.93	2.79	3.28
		out	out	2.50	3.98	4.03	3.10	3.40
4	165	in	in	2.73	4.85	4.89	3.28	3.93
		out	in	3.00	5.25	5.45	3.60	4.33
		out	out	3.15	5.41	5.68	4.26	4.63
5	201	in	in	3.28	6.30	6.72	4.29	5.15
		out	in	3.75	7.14	7.78	4.90	5.89
		out	out	4.22	7.79	8.76	6.15	6.73
6	237	in	in	3.85	8.14	9.22	5.68	6.72
		out	in	4.68	9.71	10.99	7.02	8.10
		out	out	5.63	11.49	13.66	9.34	10.03
7	274	in	in	4.86	11.03	13.45	7.86	9.26
		out	in	6.60	14.59	17.68	10.47	12.34
		out	out	9.92	21.27	27.52	17.59	19.07
8	316	in	in	6.58	15.46	20.42	11.61	13.52
		out	in	11.22	25.16	32.98	19.05	22.10
		out	out	30.07	79.62	118.33	70.41	76.48

critical plot of n versus m^{-1} was drawn, where n is the total number of fuel rods and m is the multiplication. It was recognized that the shadowing effects caused by insertion of fuel rods affected the curves of critical plot in Fig. 6. Thus, averaging the multiplication obtained by the four counters, a smooth critical plot could be obtained. A summary of multiplication observed for the cases of control rod position at each loading stage is given in TABLE 5.

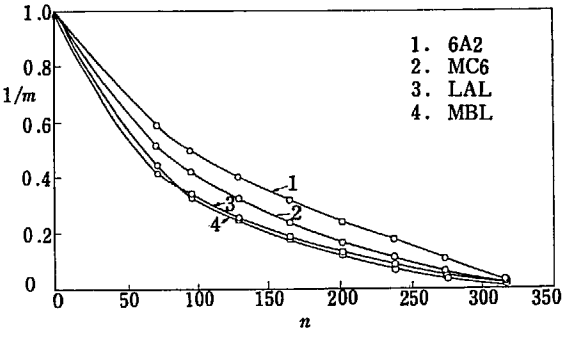

Inverse multiplication measured with each counting channels versus number of fuel rods loaded.

Fig. 6 Critical plot (1)

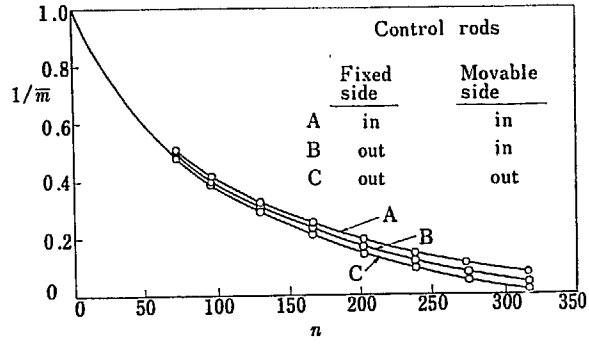

Inverse of average multiplication versus number of fuel rods loaded, at the three states of control rod positions.

Fig. 7 Critical plot (2)

For a system such as the SHE geometry, under the conditions in which the moderator was initially installed completely and fuel alone was added into the system, the approach to the rod number axis in the plot shown in Fig. 7 is shallow. The optimum loading curve is better to be a straight line, and so various forms of plots such as shown in Fig. 7 to Fig. 9 were examined. Of course, the best form of critical plot depends on the method of loading and the geometry of the system. The final plot would be arrived more or less empirically. The most successful form, which was the plot of n^{-1} versus $(m-1)^{-1}$, had an approximately linear curve except at the early stage of loading; this enabled us to perform the least square procedure of extrapolating the curve to criticality. Consequently a good prediction of the critical point was made.

A intercalibration of the reactivity worth of the control rod was made from the critical plot. It was observed that adding one fuel rod to the core-reflector boundary had a effect of 8.3 cents. By using the value and the extrapolated critical points, it was found that one control rod had a total worth of about 4.2 dollars.

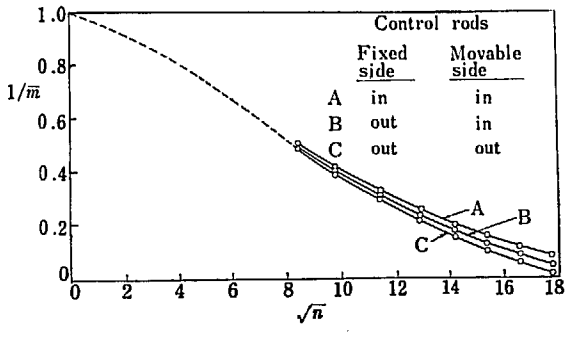

Inverse of average multiplication versus sqaure root of number of fuel rods loaded, at the three states of control rod positions.

Fig. 8 Critical plot (3)

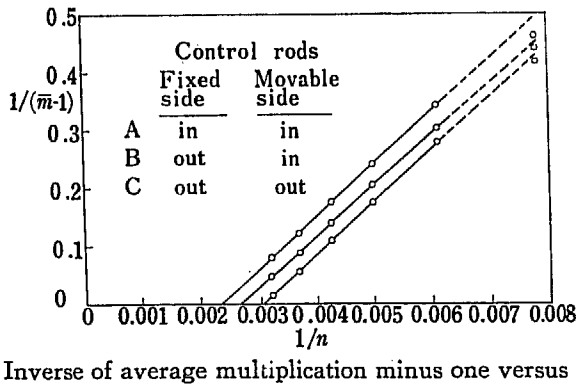

Inverse of average multiplication minus one versus inverse of number of fuel rods loaded at the three states of control rod positions.

Fig. 9 Critical plot (4)

4. Determination of the Critical Mass

Several measurements were made to determine the reactivity effects of the extraneous factors such as the holes for the safety and control rods, the residual part of the absorbing rod at the edge of reflector and the springs in the fuel rods. Consequently, the system would be reduced theoretically to the simplest form, allowing the accurate comparison of the criticality in experiments with the theoretical calculations.

Prior to the above measurements, stability checks were performed to determine whether there was any time drift of power level during the operation. The criticality was maintained at three different power levels for about 15 minutes or more, but no drift was observed during each run (TABLE 6). The results indicated that the effect of the extraneous neutron source on the criticality was negligible.

TABLE 6 Control rod positions to attain criticality at various power levels

Power level (watt)	Control rod position	
	Movable side (mm)	Fixed side (mm)
0.001	650.0	578.4
0.05	650.0	578.6
2.0	650.0	578.5

The stability of the system during short periods was satisfactory. When time proceeded, e.g., for a few days, however, setting of the control was observed to vary to a relatively large extent. No rigorous experiments were made to determine the causes, but there were found two factors which made an accurate determination of the criticality over a long period impossible. The first of these

TABLE 7 Water content in Graphite

a) Powdered sample

Sample No.	Water (%)	Measured condition	
		Temperature (°C)	Humidity (%)
1	0.079	13.5	68
2	0.061	13.5	68
3	0.070	13.5	68
4	0.071	13.0	68
5	0.061	13.0	64
6	0.054	13.0	64
7	0.064	13.0	64
8	0.080	13.0	64

b) Block sample

Sample No.	Water (%)	Measured condition	
		Temperature (°C)	Humidity (%)
9	0.07	14.0	65
10	0.05	14.0	65
11	0.07	14.0	65
12	0.09	14.0	65

factors was the moisture in the graphite, and the second was the temperature drift of the graphite. Since the air in the critical assembly room was not humidity-controlled, there was considerable uncertainty concerning the reactivity effect of the moisture in the graphite. Samples of pure graphite and fuel discs were tested and the results are shown in TABLE 7 and TABLE 8. It is seen from the data that the graphite contained as much water as about 0.09% for the pure graphite and the

TABLE 8 Water content in "U" disk

No. of measurements	Water content (%)			Measured condition	
	I	II	III	Temperature (°C)	Humidity (%)
1	0.075	0.073	0.062	15	66
2	0.071	0.068	0.055	22	42
3	0.078	0.075	0.062	18	51
4	0.076	0.073	0.059	23	49
5	0.088	0.082	0.068	11	74
6	0.082	0.077	0.062	27	35

I No coating II Single coating III Double coating

disks about 0.09%. It is appeared, however, that the graphite contained not less than about 0.1% of water on the average, since the graphite had been exposed to the atomosphere for a long time after it was installed. The temperature change in the system caused the reactivity change, which was observed by changing the room temperature. But no controlled experiments were performed.

Relative control rod positions were used as a measure of the change in reactivity introduced by the change of the system. Therefore, the control rods were calibrated by period method for the core of 333 rod loading. Several measurements as described below were performed at this loading. For the period measurement a BF_3 counter channel was used, of which the output was fed to the scaler gated to count for 18 sec and recycle in 2 sec. After the reactivity change was added, several minutes had elapsed for the transient to die out, and then a stable period was observed. The control rod calibration curves obtained are shown in Fig. 10.

Loss in reactivity due to the gap between the two halves was observed. For a given gap width the reactor was made critical by withdrawing the control rod, and the resulting reactivity change was observed. The results are shown in Fig. 11. The reproducibility of the relative position of the

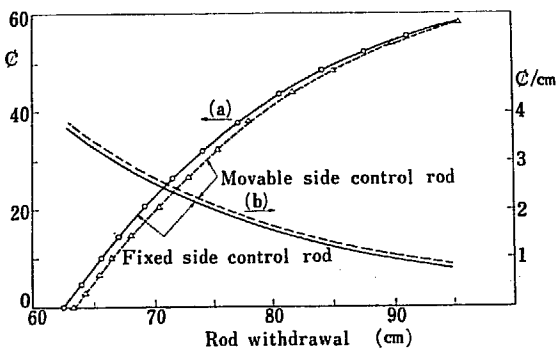

Integral (a) and differential (b) rod worth on the loading of 333 fuel rods.

Fig. 10 Control rod calibration

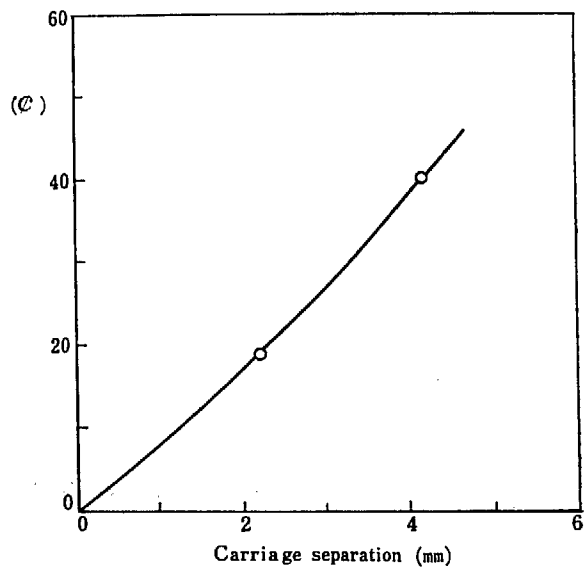

Reactivity effect of the gap between two half assemblies.

Fig. 11 Gap effect

movable half against the fixed one was measured, and was found to be within about ±0.01 mm. Thus the reactivity change due to the mechanical reproducibility may be small.

Eight holes, which extended from the center of the core to the outer edge, were left unloaded in the matrix for the control and safety rod mechanisms. Insertion of the fuel rod into the hole increased the amount of fuel in the core and reduced the loss of neutrons by streaming, of which effects were observed in the following manner. One fuel rod was removed from the position corresponding to that of control rod in another section of the 60° co-ordinate system, and the reactivity change was observed to be 25.7 cents. The same procedure was also used for the safety rods, and the result was 21.2 cents. The difference between the values was due to the different importance between the two positions.

At the outmost positions, both the control and safety rods remain 30 cm in the reflector. The poisoning effect of the remaining part was determined by insertion of an absorbing rod which was identical with the control or safety rods. The poisoning effect was small; the results were 5.5 cents for the control rod and 4.1 cents for the safety rod. The perturbation of the flux by the holes and by the remaining parts of the rods was small. Thus the interactions were neglected.

The spring in the fuel rod resulted in the increase of neutron absorption. The poisoning effect of the spring at the center of the core was observed. By using the results it was estimated that the springs introduced a total reactivity change of about 15.1 cents.

The effectiveness of the fuel rod near the core boundary was determined by replacing one fuel rod with a dummy rod. Precisely, the results included the effect from the small change in the amount of graphite; the overall effect was 8.3 cents per rod.

The results of critical mass determination, taking into account all the effects already mentioned, are given in TABLE 9. The results have an error of ±1.5 fuel rods. Observation of the effects of

TABLE 9 Reactivity effects and criticality data

Reactivity effects	Measured value (¢)	Calculated value (¢)
Holes for control rods	−25.7±0.4	
Holes for safety rods	−21.2±0.6	
Remaining parts of control rods	−5.5±0.7	7.2
Remaining parts of safety rods	−4.1±0.5	
Springs	−15.1	19
Fuel rod (in "8" layer)	+8.3	
Gap	∼ −7/mm	

Criticality data	
Number of fuel rods	298.4 rods
Critical mass of ^{235}U	3.074 kg

the void and imhomogeneity was not made, but the effects may be small when considering the measured flux distribution in the fuel rod and theoretical analysis. The effects of a tephlon coating of the fuel disks and of impurities in the core materials were ignored.

5. Flux and Power Distributions

The macroscopic neutron flux distribution in the assembly and microscopic distribution in the fuel rods were measured using various kinds of foils. The power distribution in the core was measured with a fission counter. In order to measure the macroscopic neutron flux distribution,

copper and indium foils were inserted, directly or with alumium foil-holder, into the gaps made by the piled-up tubes and rods, and irradiated. The induced activities of the foils were measured with Geiger-Mueller counters.

As the activation cross section of ^{63}Cu obeys the $1/v$ law up to a fairly high energy region*, the measured activity of copper foils, with a half life of 12.8 hr, corresponds nearly to the total neutron density**. Radial distribution in the central plane measured along the diagonal direction and the direction perpendicular to one side of the hexagon are shown in Fig. 12 and Fig. 13. The

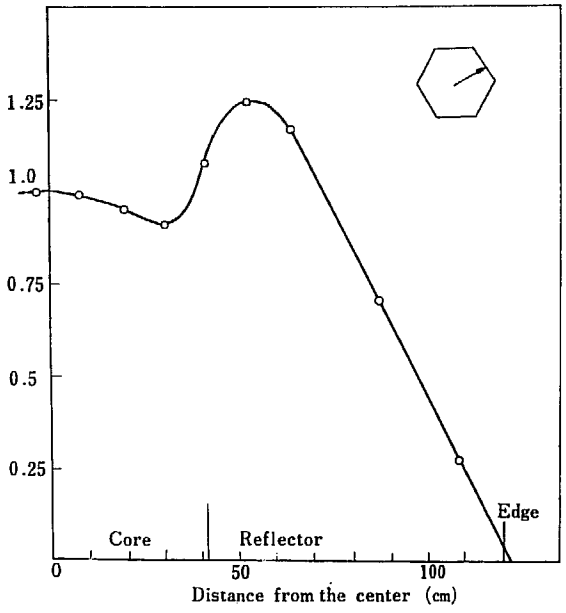

Fig. 12 Neutron distribution measured with copper foils, along the radial direction indicated in the accompanying figure in the central, cross-sectional plane.

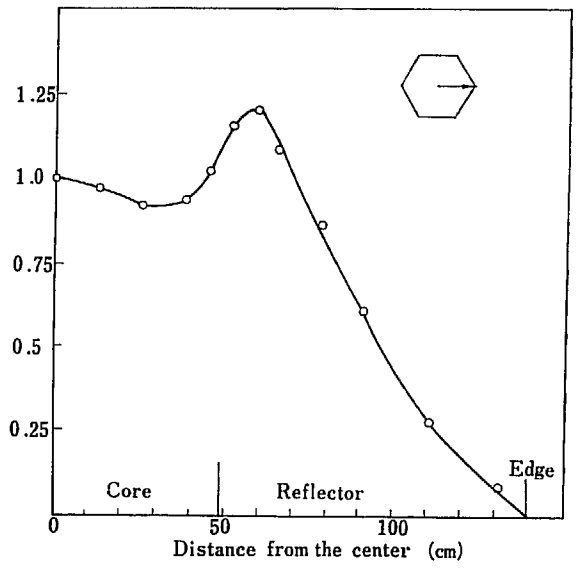

Fig. 13 Neutron distribution measured with copper foils, along the radial direction indicated in the accompanying figure in the central, cross-sectional plane.

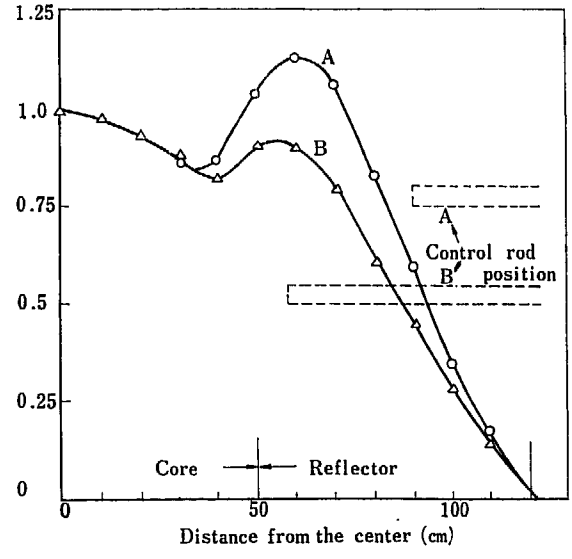

Fig. 14 Neutron distribution measured with copper foils, along the central axis. The effect of control rod position is shown in two curves.

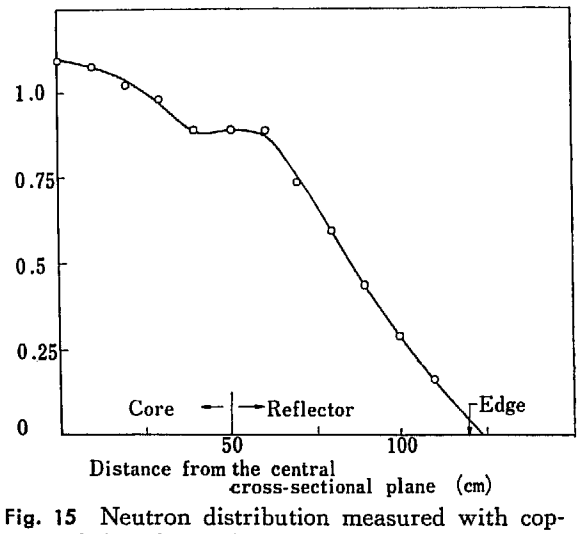

Fig. 15 Neutron distribution measured with copper foils, along the boundary of core and reflector.

* The first resonance of ^{63}Cu appears in 580 eV.

** The fact that the measured cadmium ratios at the center of the assembly are about 10 for BF_3 counter and about 5 for ^{63}Cu, shows that the above statement is not strict.

copper activation at the core center is normalized to unity. Comparing these two distributions, it is evident that the width of the reflector peaking of the neutron density in the direction perpendicular to the side of hexagon is wider than the one along the diagonal direction. This is attributed to the effect of the hexagonal shape of the core. The axial distributions measured along the central axis and the boundary of the core and reflector are shown in Fig. 14 and Fig. 15. The effect of the position of the control rod which moves through the hole about 10 cm from the central axis is seen in Fig. 14. The diagonal distribution in the horizontal cross sectional plane which passes through the core center is shown in Fig. 16. From the distributions given above the contour map of the neutron density on the horizontal cross sectional plane is plotted in Fig. 17, which is considerably different from the counterpart in the spherical system. The similar distributions measured with BF_3 counter also given in Fig. 18 and Fig. 19. The epi- and sub-cadmium

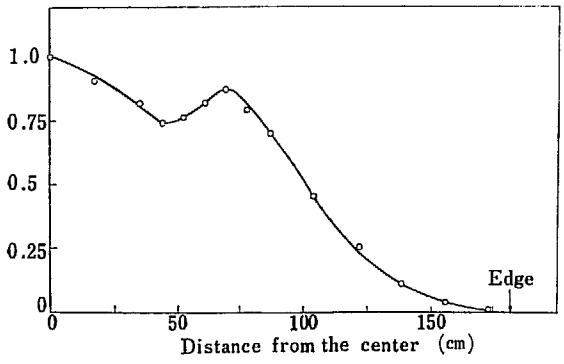

Fig. 16 Neutron distribution measured with copper foils, along the diagonal direction in the horizontal cross-sectional plane.

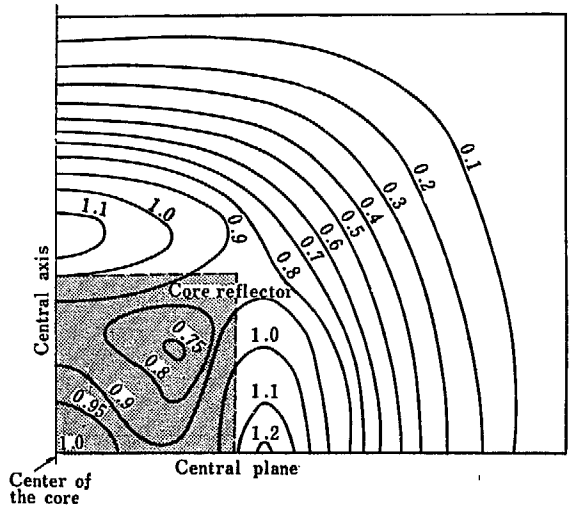

Fig. 17 Contour map of neutron distribution measured with copper foils in a quater of the horizontal cross-sectional plane.

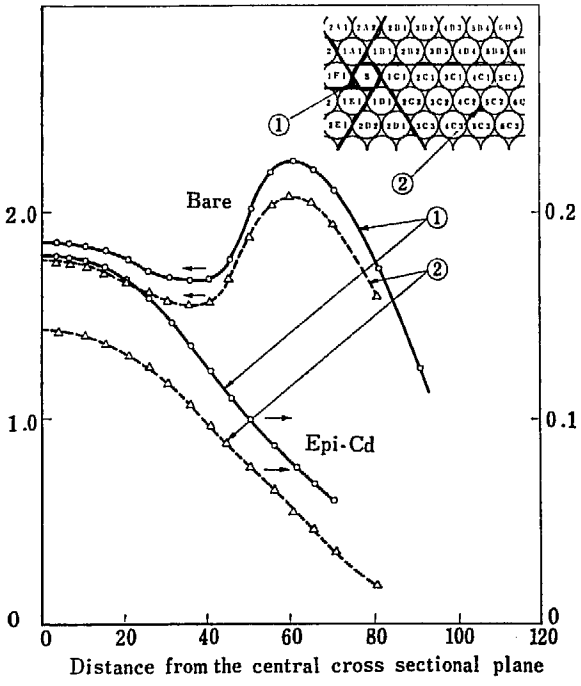

Fig. 18 Neutron distribution measured with BF_3 counter along the axial direction.

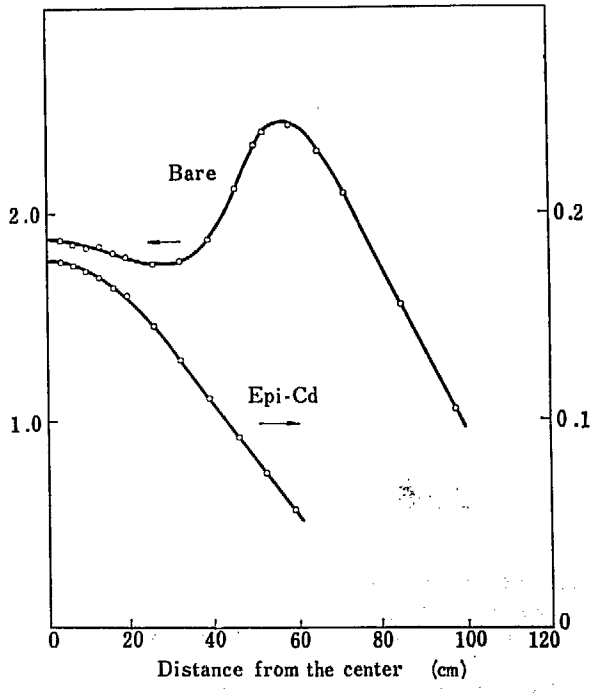

Fig. 19 Neutron distribution measured with BF_3 counter along the radial direction.

neutron densities were measured with indium foils, using cadmium covers. The thickness of the indium foils and cadmium covers was 30 mg/cm² and 0.5 mm, respectively. The measured activities of the bare and cadmium-covered indium foils are shown in Fig. 20 and Fig. 21 for the radial direction and for the central axis. The distributions of the ratios of the epi-cadmium to sub-cadmium neutron densities were calculated from the measured distributions just given and from the known values of the thermal cross section and resonance integral of indium. In the calculation, corrections were made for the self-shielding for the neutron capture and for the self-absorption for the β-rays, according to GREENFIELD's data[1]. The results are shown in Fig. 22 and Fig. 23.

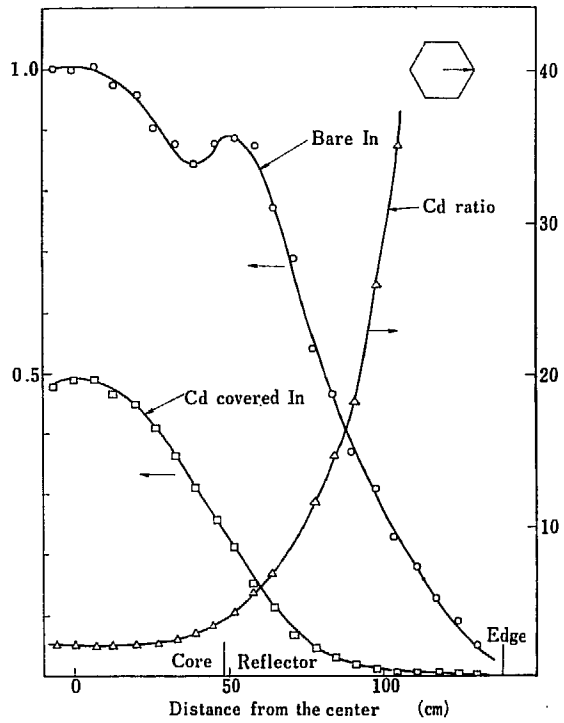

Fig. 20 Variation of bare and cadmium-covered indium activities and cadmium ratios along the radial direction indicated in the accompanying figure.

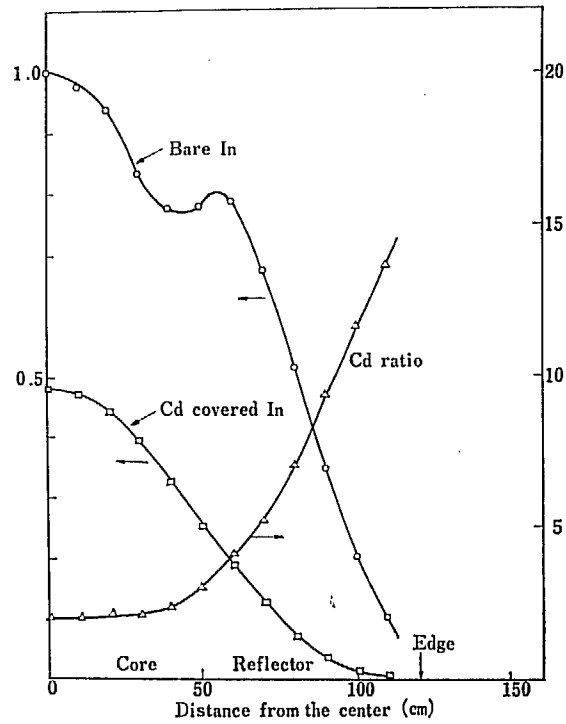

Fig. 21 Variation of bare and cadmium-covered indium activities and cadmium ratios, along the central axis.

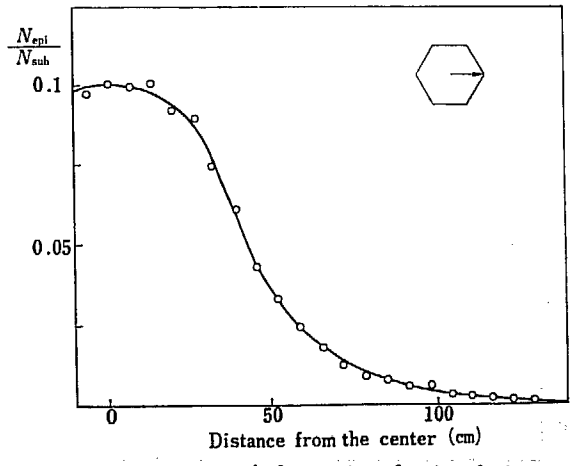

Fig. 22 Variation of the ratio of epi-cadmium to sub-cadmium neutron density deduced from the cadmium ratio of indium, along the radial direction indicated in the accompanying figure.

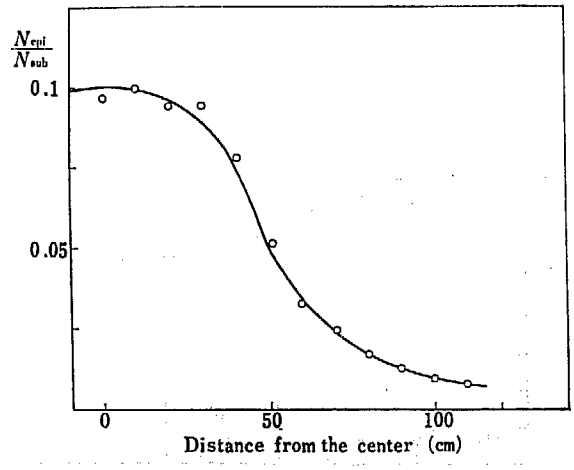

Fig. 23 Variation of the ratio of epi-cadmium to sub-cadmium neutron density deduced from the cadmium ratio of indium, along the central axis.

The core of SHE consists of a assembly of double graphite tubes, i. e., the matrix tube and the fuel sheath, and disks which fill the inner tubes. The thickness of the two tubes is 5 mm. Three kinds of disks; i. e., "U", "1" and "5" disks, were used for the SHE-I core. The diameter of the disks was 45 mm and the thicknesses were 10 mm, 10 mm and 5 mm, respectively. The "U" disks were a mixture of UO_2 and graphite, and the "1" and "5" disks graphite. With this semi-homogeneous structure, the neutron flux has a fine structure. The microscopic thermal flux distribution was measured using dysprosium micro-foils and the disadvantage factor in calculating the thermal utilization factor was given. The foils were a mixture of powdered dysprosium oxide (Dy_2O_3) and polyethylene, and were 2 mm in diameter and about 0. 5 mm in thickness. The foil

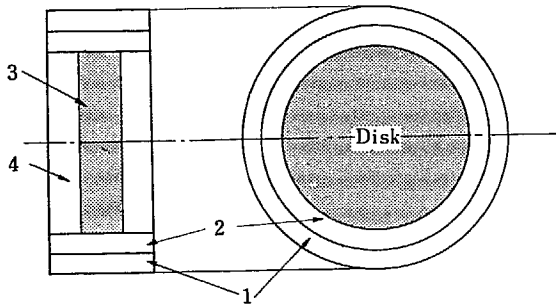

1. Matrix tube
2. Fuel sheath
3. U disk
4. Graphite disk

Fig. 24 Unit cell in the fine stucture distribution.

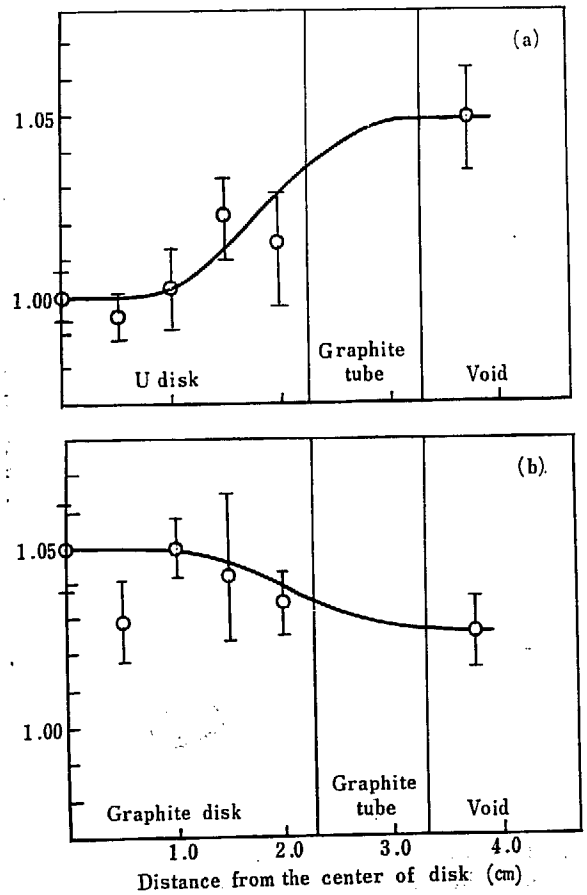

Fig. 25 Fine structure distributions along the radial direction in U disk (a) and graphite disk (b).

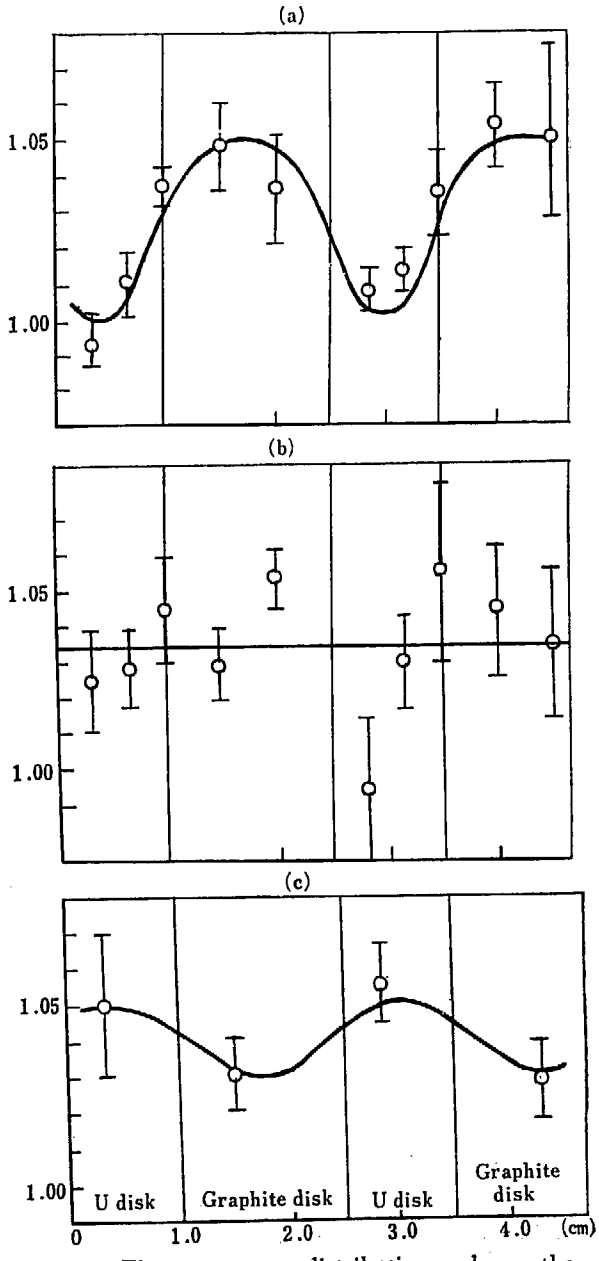

Fig. 26 Fine structure distributions along the central axis of fuel rod (a), along the edge of disk (b) and along the void channel (c).

contained about 1 mg of dysprosium oxide. The relative sensitivity of each foil was calibrated by irradiating in the JRR-1 thermal column. The unit cell for the fine structure distribution in the SHE-I core is shown in **Fig. 24.** To measure the distribution in the disks, the "U" disk was replaced by three thin disks, which were the same as the "U" disks except in thickness; 3.5 mm. The "1" disks were replaced by two "5" disks. Small holes were made on the surfaces of the disks in which foils were placed. The fine structure was observed along the radial and axial directions. The results of measurements are shown in **Fig. 25** and **Fig. 26**, where the dysprosium activations are normalized to unity at the center of the "U" disk. Two radial distributions measured along the directions toward the void and toward the point of contact with the neighboring rod showed no significant difference and their average is shown in the figure. The radial distribution in the "U" disk and the axial distribution along the central axis of the fuel rod showed an approximately five percent depression. The radial distribution in the graphite disk and the axial distribution in the void showed slightly opposite variations, but this is indefinite due to the experimental errors. The disadvantage factor for the thermal neutron flux distribution is defined as

$$D = \frac{\text{Average thermal neutron flux in the pure graphite part } (\Phi_G)}{\text{Average thermal neutron flux in the U disk } (\Phi_U)} \quad \cdots\cdots\cdots (1)$$

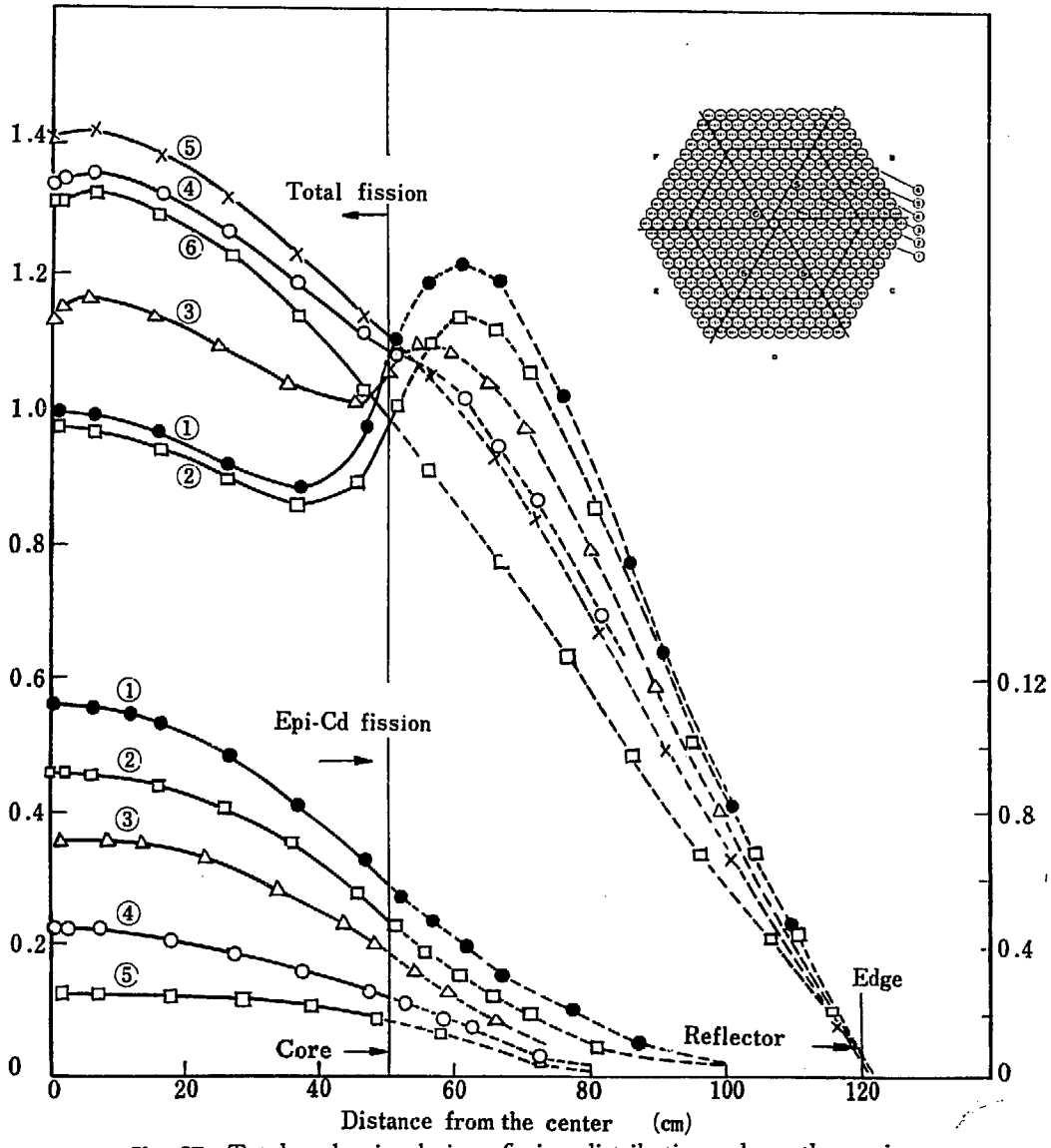

Fig. 27 Total and epi-cadmium fission distributions along the various axes indicated in the accompanying figure.

Then the thermal neutron utilization factor,

$$f = \frac{Z_U V_U}{\Sigma_U' V_U + \Sigma_G' V_U + D\Sigma_G V_G} , \quad \cdots\cdots (2)$$

where V_G and V_U are the volumes of the pure graphite and the "U" disk, Σ_G and Σ_G' are the macroscopic cross sections of graphite in both parts and Σ_U is of uranium in the "U" disk. The distribution of the dysprosium activation do not exactly correspond to the thermal neutron distribution, but because of the relatively small resonance absorption of dysprosium the former was regarded as equivalent to the latter. The measured distribution was volume-integrated in the unit cell to give the average thermal neutron fluxes, $\Phi_U = 1.02$ and $\Phi_G = 1.04$, from which the disadvantage factor was given as $D = 1.02$. From this value the error in the thermal utilization factor, $\Delta f/f$, in the treatment of the system as homogeneous was estimated as about 7×10^{-4} for the SHE-I, where f is 0.957. Thus the core may be reasonably treated as homogeneous with regard to the thermal neutron absorption*.

The fission distribution of ^{235}U, i.e., power distribution, was measured with a small fission counter, which was a FC 4/1000 type, made by 20 th Century Co., the diameter of which was 0.64 cm and the effective length 2.54 cm. The counter traversed the void channel axially and the specially provided channel radially by the drive mechanism. The position of the counter was indicated by means of selsyns. The power level of the reactor was normalized with a BF_3 counter throughout the measurement. The epi-cadmium fission distribution was measured, with the counter covered with a 0.5 mm thick cadmium cover. The axial distribution in the fixed half is shown in Fig. 27, with the positions of the axes being indicated in the accompanying figure. The distribution along the central axis could not be observed, due to the obstacle of the control rod drive mechanism. The decrease in the distribution No. 3 near the central plane was attributed to the neutron absorption of the fuel rod, loaded additionally in the "8" layer of the movable half. In the Fig. 28 the radial distribution is shown.

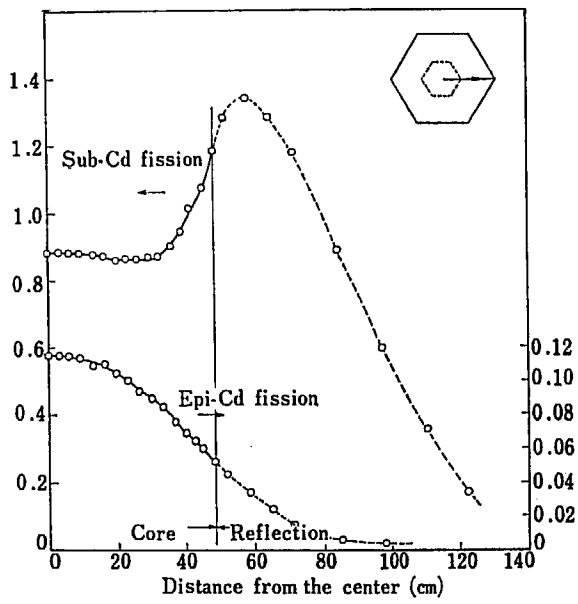

Fig. 28 Sub- and epi-cadmium fission distribution along the radial direction indicated in the accompanying figure.

* The recent experimetal results indicated that the heterogeneity exists for resonance absorption in ^{238}U.

6. Calculation of the Neutron Spectrum

As mentioned already, the neutron leakage is quite appreciable in an enriched-uranium, graphite-moderated system. The neutron leakage is more sensitive to the shape of the neutron spectrum. In the type of system under consideration the thermal diffusion area is much smaller than the slowing-down area; thus the fast leakage is larger than the thermal leakage. In the thermal reactors the usual approximation is made by the Maxwellian distribution plus a $1/E$ tail. But it is considered desirable that the neutron spectrum is more adequately described. The calculation of the neutron spectrum consists of two steps; the first is to determine the fast neutron spectrum and the other the thermal neutron spectrum. The nuclear behavior in the system is approximated by the homogeneous system.

For the graphite-moderated thermal reactor, the age theory is sufficiently accurate, but the fast neutron spectrum is distorted from the $1/E$ distribution by relatively large neutron absorption and leakage. Thus the fast neutron spectrum was calculated by the multigroup approximation of the age-diffusion theory and by using an assumed fission neutron source distribution. When the system contains hydrogen, the age diffusion equation may be improved by taking into account the hydrogen slowing-down by the Geortzel-Selengut treatment. The age-diffusion equation can be written as

$$D\nabla^2\phi-\Sigma_a\phi-\frac{\partial q}{\partial u}-\frac{\partial q_H}{\partial u}+S=0 \quad \cdots\cdots(3)$$

$$\frac{\partial q_H}{\partial u}+q_H-\Sigma_H\phi=0 \quad \cdots\cdots(4)$$

where ϕ is the neutron flux per unit range of lethargy u; q is the slowing-down density, and q_H is the hydrogen slowing-down density. Σ_a and Σ_H are the total absorption cross section and the hydrogen scattering cross section, respectively. The source, S, represents neutrons liberated in the fission. Inelastic scattering of the fast neutrons by uranium was disregarded. The procedures for obtaining the multigroup equations from the age-diffusion equations have been described in many literatures. In the present calculation the scheme-A was used.

The absorption and fission cross sections in the groups should be replaced by the cross sections averaged with the neutron spectrum. The average uranium cross sections were calculated considering the finite dilution. The resonance parameters are well-known up to about 35 eV for ^{235}U and up to about 500 eV for ^{238}U. The sum of the contributions from the resonance levels of the heavy elements to the effective resonance integral was calculated. Unfortunately, in some energy regions the cross section data of the heavy elements are not known with sufficient accuracy.

The average fission cross sections of ^{235}U are nearly $270\,E^{-0.5}$ from 35 eV to 2 keV and $60\,E^{-0.305}$ from 2 keV to 200 keV. Above 200 keV it was assumed to be constant, i.e., 1.2 b. Because of the uncertainty in the value $\alpha(E)$, the fission to capture ratio, of ^{235}U in the resonance energy region, the average value of $\alpha(E)$ was assumed to be 0.3 in the present calculation. For the ^{238}U cross section there are no available data for the energy region from 1 keV to 10 keV, and so a statistical model was adopted in the region. From the cross section data the effective resonance integral of ^{235}U became to be 262.2 barns, while the capture resonance integral of ^{238}U 170.8 barns.

The thermal neutron spectrum was calculated by using a crystal model of graphite, in which the emission and absorption of the vibrational quanta in the collision process were considered. Experimental information on the thermal spectrum in graphite is limited, but it is known that the chemical binding reduces the energy transfer between neutrons and carbon nucleus[2]. It has been indicated by experiments that the effective value of the average logarithmic energy decrement in

the graphite is considerably smaller than for free carbon moderator in the thermal energy region. Then the thermal neutron spectrum in the graphite-moderated reactors is expected to be much hardened.

The energy transfer cross section $\sigma(E\to E')$ in the graphite was calculated, using two approximations, i. e., phonon expansion for a low energy neutrons and short time collision approximations for high energy neutrons[3]. Two models of phonon frequecy distribution were used in the case of graphite which has a layer structure; one for the vibrations normal to the layers was a complicated BALDOCK's model and another vibration in the layers a more simple KRUMHAUSL-BROOKS model. The interaction between these modes was neglected. For the graphite crystal model, the resulting expression for the momentum transfer cross section $\sigma(\vec{p}\to\vec{p}')$ per carbon nucleus for the single crystal in incoherent approximation is

$$\sigma(\vec{p}\to\vec{p}')=\frac{\sigma_0}{8\pi^2\hbar}\left(\frac{p'}{p}\right)\int_{-\infty}^{\infty}e^{-\frac{1}{\hbar}(E'-E)t}\exp[\Delta p_\perp{}^2\{W_\perp(t)-W_\perp(o)\}+$$
$$+\Delta p_\parallel{}^2\{W_\parallel(t)-W_\parallel(o)\}]dt \quad\cdots\cdots(5)$$

where

$$W_\perp(t)=\frac{\hbar}{2M}\int\rho_\perp(\omega)\left\{e^{-i\omega t}+\frac{2\cos\omega t}{\exp(\hbar\omega/\kappa_0 T)-1}\right\}\frac{d\omega}{\omega}$$
$$W_\parallel(t)=\frac{\hbar}{2M}\int\rho_\parallel(\omega)\left\{e^{-i\omega t}+\frac{2\cos\omega t}{\exp(\hbar\omega/\kappa_0 T)-1}\right\}\frac{d\omega}{\omega}$$

Here $\vec{p}$ and E are the initial momentum and energy, $\vec{p}'$ and E' are the final momentum and energy of the neutron, σ_0 is the scattering cross section of the bound nucleus, $\Delta p_\perp$ and $\Delta p_\parallel$ are the perpendicular and parallel components to the crystal plane of the momentum change $\Delta\vec{p}=\vec{p}'-\vec{p}$, M is the mass of the carbon nucleus, ω is the angular frequency of the quanta, and $\rho_\perp(\omega)$ and $\rho_\parallel(\omega)$ are the frequency distributions of the transverse and planer modes, respectively. The n-quantum differential cross section is obtained by expanding the second exponential function of Eq.

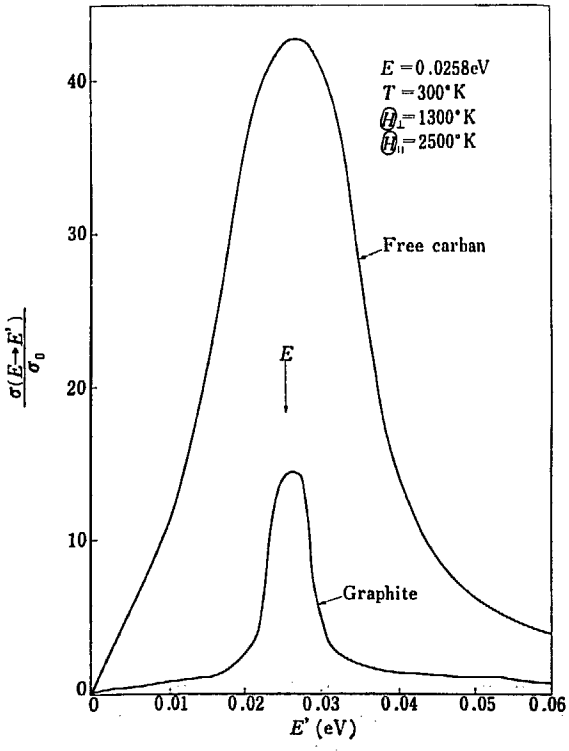

Fig. 29 Energy transfer cross section of graphite moderator calculated by phonon expansion including up to six phonon terms.

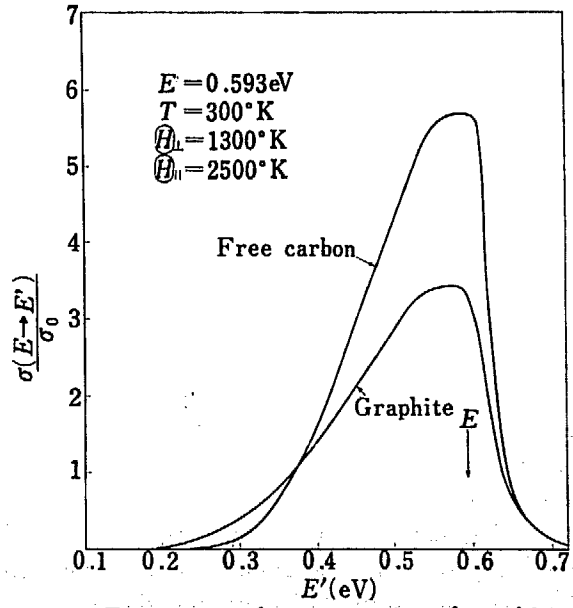

Fig. 30 Energy transfer cross section of graphite moderator calculated by using the short time collision approximation.

(5) and integrating the n-th order term over t. For large neutron energy a short time collision approximation is used. $W_{\perp}(t)$ and $W_{\parallel}(t)$ were expanded in powers of t, and retained up to t^2 order terms. In this approximation the time integration is easily performed. The final cross section required for the spectrum calculation was the energy transfer cross section for polycrystal. Hence the integration over the scattering angle of the neutron and the averaging over the orientation of the crystal plane were performed. In Fig. 29 and Fig. 30, $\sigma(E \to E')$ is plotted as a function of final neutron energy E' for two values of E.

Althouth the reactor under consideration is of two region, the spatial dependence of the thermal neutron spectrum was ignored. Consequently, the thermal neutron spectrum for the infinite homogeneous medium was calculated for simplicity. The integral equation for the thermal neutron spectrum was numerically solved. It is of interest to compare the results with those for free carbon moderator. The spectra calculated in the SHE-I core, as well as the fast neutron spectra, are shown in Fig. 31, for the same value of neutron absorption, 130 mb per carbon atom.

To illustrate the effect of the chemical binding in the graphite on the criticality, the reactivity difference between two types of reactor, i. e., graphite and free carbon moderated reactors, was

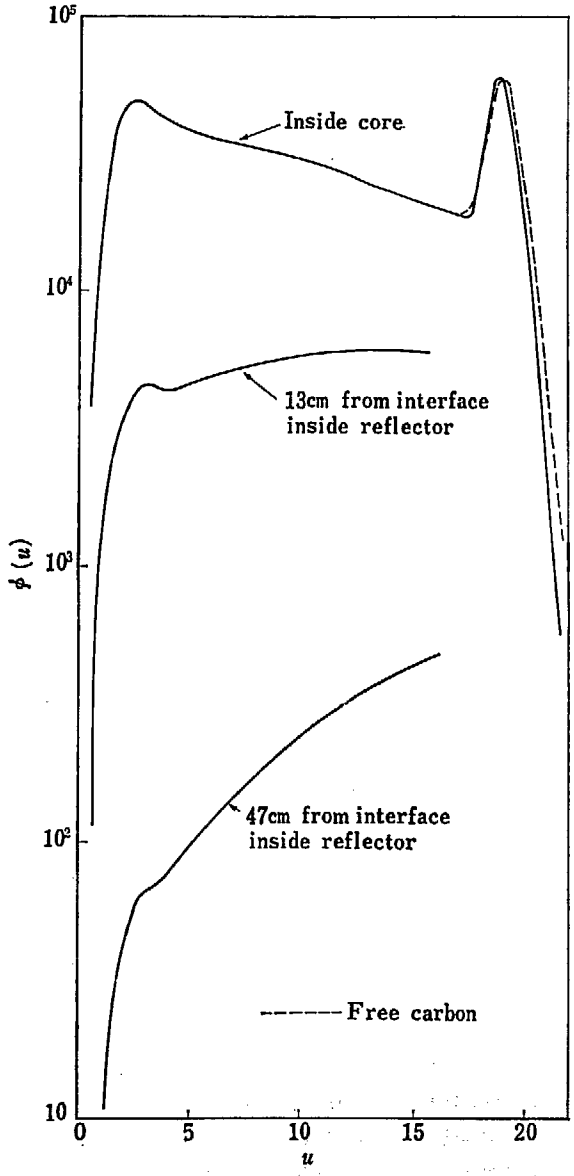

Fig. 31 Calculated neutron flux distribution in SHE-I.

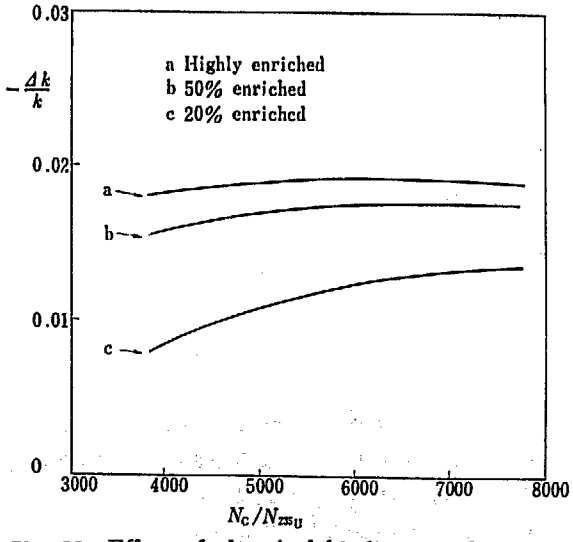

Fig. 32 Effect of chemical binding on the reactivity.

calculated for various enrichments. It was assumed that the reactors were both bare and homogeneous, and the chemical binding affected only the thermal group. The reactivity change due to the chemical binding is given by

$$\frac{\Delta k_{\text{eff}}}{k_{\text{eff}}} = \frac{\Delta \eta f}{\eta f} - \frac{B^2 \Delta L^2}{1+B^2 L^2} \quad \cdots\cdots (6)$$

where ηf is the thermal value, B^2 is the critical buckling and L^2 is the thermal diffusion area. The chemical binding in the crystal makes the average velocity of the thermal neutrons increase, then the thermal neutron leakage from the core increases. This effect is given by the second term in Eq. (6), and is larger than the first term. The results are shown in Fig. 32 for various enrichments and concentrations.

7. Criticality Calculation

Criticality calculation was made by using the multigroup approximation of the age-diffusion equation. The fundamental criticality equations used were Eqs. (4) and (5) supplemented by the equations for the thermal neutron group. A two-dimensional, machine multigroup calculation was not available in the present work, and so all of the machine calculations were based on the one-dimensional reactor model. Since SHE is a hexagonal prism, the use of a one-dimensional model was not so adequate. It was assumed, however, that the actual hexagonal reactor had the same neutron multiplication as a spherical reactor with 5% less core volume. In general, the cross section from BNL-325 were used and the average cross section were calculated using the spectra obtained in the preceding chapter. Inelastic scattering were neglected. The transfer cross section from the epithermal group to the thermal group was obtained from the logarithmic energy decrement in the free carbon moderator and from the calculated spectrum.

The hypothesis of the group approximation, that the neutron spectrum of each group is independent of the position, breaks down in the reflector. Therefore, for the fast neutron group, the reflector was divided into three regions. The neutron temperature is of importance in determination of thermal leakage. The thermal diffusion coefficient is proportional to the mean thermal velocity, whereas the absorption rate in the near $1/v$ absorbers is almost spectrum-independent. The effective neutron temperature in the core varies appreciablly near the core-reflector boundary, and it will tend to be equal to the physical temperature of the graphite in the reflector. In the present calculation the effective neutron temperature in the reflector was arbitrarily made equal to the reflector temperature.

The energy groups and the average cross sections for the core and reflector are given in TABLE 10. In the equivalent spherical model, the core radius was 49.9 cm and the reflector radius

TABLE 10(a) Multigroup constants

Group	Range in u	Lower energy limit	Fission spectrum	Core constants				
				D	Σ_a	Σ_F	Σ_{Sl}	Σ_{SH}
1	0 — 1.0	3.678 MeV	0.1314	2.673	0.0000234	0.0000179	0.07054	0.000172
2	1.0— 2.0	1.353 MeV	0.4415	2.395	0.0000244	0.0000187	0.03611	0.000296
3	2.0— 3.0	497.7 keV	0.2951	1.634	0.0000234	0.0000176	0.03900	0.000490
4	3.0— 4.0	183.2 keV	0.0987	1.174	0.0000268	0.0000197	0.04850	0.000816
5	4.0— 7.0	91.19 keV	0.0329	0.9969	0.0000564	0.0000350	0.01788	0.001592
6	7.0—10.0	4.540 keV	0.0004	0.9745	0.0003413	0.0000993	0.01823	0.002040
7	10.0—13.2	150.3 eV	—	0.9773	0.001965	0.0004570	0.01368	0.002102
8	13.2—16.865	0.474 eV	—	0.9694	0.001963	0.0005376	0.01501	0.002173
9	thermal	—	—	0.9425	0.006576	0.005209	—	—

TABLE 10(b) Multigroup constants

Group	Reflector-1 constants				Reflector-2 constants			
	D	Σ_a	Σ_{SI}	Σ_{SH}	D	Σ_a	Σ_{SI}	Σ_{SH}
1	2.540	—	0.08507	0.000176	2.522	—	0.08067	0.000176
2	2.388	—	0.03759	0.000297	2.388	—	0.03751	0.000294
3	1.634	—	0.03992	0.000490	1.634	—	0.03951	0.000490
4	1.172	—	0.05059	0.000818	1.172	—	0.05050	0.000819
5	0.9948	—	0.02002	0.001612	0.9934	—	0.02213	0.001626
6	0.9747	—	0.01990	0.002042	0.9148	—	0.02181	0.002045
7	0.9773	—	0.01827	0.002103	0.9773	—	0.02020	0.002103
8	0.9691	—	0.01624	0.002175	0.9686	—	0.01795	0.002177
9	0.9474	0.000306			0.9474	0.000306		

TABLE 10(c) Multigroup constants

Group	Reflector-3 constants				f_{core}	$f_{reflector\text{-}1}$	$f_{reflector\text{-}2}$	$f_{reflector\text{-}3}$
	D	Σ_a	Σ_{SI}	Σ_{SH}				
1	2.522	—	0.03719	0.000176	0.24 *	0.20	0.20	0.19
2	2.389	—	0.03790	0.000297	0.65	0.63	0.63	0.62
3	1.634	—	0.03921	0.000490	0.88	0.86	0.87	0.88
4	1.172	—	0.05126	0.000819	0.99	0.95	0.95	0.93
5	0.9935	—	0.02213	0.001625	1.05	0.93	0.85	0.95
6	0.9748	—	0.02285	0.002046	1.05	0.96	0.88	0.84
7	0.9773	—	0.02116	0.002103	1.07	0.98	0.89	0.85
8	0.9682	—	0.01888	0.002178	1.05	0.97	0.88	0.83
9	0.9474	0.000306						

* f factor is $\bar{q}_i/q_i^\circ$, where q_i° is the slowing down density at the low energy limit of the i-th group and $\bar{q}_i$ is the average value of the slowing-down density in the i-th group.

TABLE 11 SHE-I composition

Constituent	Core	Reflctor
^{235}U	0.1439×10^{20} /cm^3	——
^{238}U	0.5739×10^{20}	——
Carbon	774.1×10^{20}	774.1×10^{20}
Hydrogen	1.032×10^{20}	1.032×10^{20}
Oxgen	1.953×10^{20}	0.5161×10^{20}
Nitrogen	0.088×10^{20}	0.088×10^{20}

TABLE 12 Summary of criticality calculations

Case	ν_c
I (1)	2.461
II (2)	2.465
III (3)	2.450
III (4)	2.406

(1) The actual equivalent reactor*, 9 groups.
(2) Same as I except that the moisture is not included.
(3) Same as I except that the air is not included.
(4) Same as I except the thermal group constants in free carbon moderator.

* The average moisture in the graphite is 0.1%.

140.5 cm. The composition of the equivalent spherical reactor is listed in TABLE 11. A summary of the multigroup calculations is given in TABLE 12. As mentioned already, the graphite contains a considerable amount of moisture. The effect of moisture on the reactivity was calculated for various content of moisture in the graphite, and the results are shown in Fig. 33. The presence of moisture in the graphite increase the reactivity by about 0.2% for the SHE-I. The relation between the reactivity and the critical mass is given approximately as

$$\Delta k/k = (1/4.7)(\Delta M/M) \quad \cdots\cdots (7)$$

for the SHE-I core system.

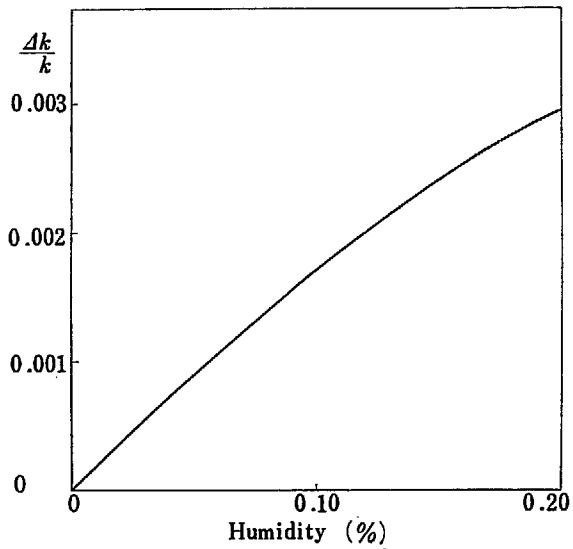

Fig. 33 Reactivity change due to the moisture in the graphite.

8. Conclusions

The graphite-moderated critical assembly is well suited for the study of clean and cold graphite-moderated systems, since no structural materials other than graphite are used in the core. The experimental results serve to confirm the present approach and existing methods of calculation, and the results obtained demonstrate the feasibility of the approach in a limited area such as in the case of graphite-moderated enriched-fuel reactors. The multigroup treatment gives a satisfactory description of a small thermal system. The calculated value of ν_0 is 2.461, while the latest accepted value of ν is 2.43 ± 0.02. From the Eq. (7), the calculated critical mass is within about 6% of the experimental value. This may be considered a satisfactory agreement in this small reactor. It is expected that the procedure proposed can be used with some degree of confidence to calculate the criticality data for the system under consideration without using the results of the integral experiments.

Since SHE-I has a finite core and a large reflector, the effect of the chemical binding in reducing reactivity is such as a one as to make the calculated criticality too small. The results are also considerably sensitive to the constants for high energy groups. Then this energy region should be treated with more attention. The remainder of the difference in ν may be ascribed to the use of age theory and treatment of the resonance absorptions. In the future experiments, deficiency associated with the two-dimensional geometry of the system will be eliminated by removing the end reflectors of the SHE facility, and the calculation will be performed with more correct geometry.

Acknowledgement

The authors wish to express particular thanks to Dr. W. Y. KATO for many suggestions and advices, to Dr. E. NISHIBORI for encouragement during the cource of this work, and to Dr. A. SUGIMOTO and Dr. A. TAKEDA for supporting the research.

Finally, they also wish to thank Miss. A. ODAKURA for the numerical computations.

References

1) M. A. GREENFIELD: *Nuclear Sci. and Eng.*, **2**, 246 (1957)
2) A. W. MCREYNOLDS *et al.*: P/1540, Second International Conference on the Peaceful Uses of Atomic Energy, Geneva, 1958. B. N. BROCKHOUSE and D. G. HURST: *Phys. Rev.*, **88** 542 (1952)
3) K. INOUE: to be published